# Observation of double-well potential of NaH C $^1\Sigma^+$ state: Deriving the dissociation energy of its ground state

Chia-Ching Chu, Hsien-Yu Huang, Thou-Jen Whang, and Chin-Chun Tsai

Citation: The Journal of Chemical Physics **148**, 114301 (2018); doi: 10.1063/1.5020827
View online: https://doi.org/10.1063/1.5020827
View Table of Contents: http://aip.scitation.org/toc/jcp/148/11
Published by the American Institute of Physics



# Observation of double-well potential of NaH $C\ ^1\Sigma^+$ state: Deriving the dissociation energy of its ground state

Chia-Ching Chu,[1,a)] Hsien-Yu Huang,[1,a)] Thou-Jen Whang,[1,b)] and Chin-Chun Tsai[2,b)]
[1]*Department of Chemistry, National Cheng Kung University, Tainan 70101, Taiwan*
[2]*Department of Physics, National Cheng Kung University, Tainan 70101, Taiwan*

(Received 27 December 2017; accepted 21 February 2018; published online 15 March 2018)

Vibrational levels ($v$ = 6–42) of the NaH $C\ ^1\Sigma^+$ state including the inner and outer wells and the near-dissociation region were observed by pulsed optical-optical double resonance fluorescence depletion spectroscopy. The absolute vibrational quantum number is identified by comparing the vibrational energy difference of this experiment with the *ab initio* calculations. The outer well with $v$ up to 34 is analyzed using the Dunham expansion and a Rydberg-Klein-Rees (RKR) potential energy curve is constructed. A hybrid double-well potential combined with the RKR potential, the *ab initio* calculation, and a long-range potential is able to describe the whole NaH $C\ ^1\Sigma^+$ state including the higher vibrational levels ($v$ = 35–42). The dissociation energy of the NaH $C\ ^1\Sigma^+$ state is determined to be $D_e(C)$ = 6595.10 ± 5 $cm^{-1}$ and then the dissociation energy of the NaH ground state $D_e(X)$ = 15 807.87 ± 5 $cm^{-1}$ can be derived. *Published by AIP Publishing.* https://doi.org/10.1063/1.5020827

## I. INTRODUCTION

Sodium hydride, which is one of the simplest electronic structures among the neutral heteronuclear molecules, has constantly been investigated for comparison between experiment and theoretical calculation. Even though it was widely investigated, there are only a few electronic states that have been experimentally observed. The most focused ground state ($X\ ^1\Sigma^+$) and two low-lying excited states ($A\ ^1\Sigma^+$ and $C\ ^1\Sigma^+$) have been reported. The difficulty is that the ionic-covalent avoided crossing between the $X\ ^1\Sigma^+$ and $A\ ^1\Sigma^+$ states results in an aberrant behavior for the potential curves of both low-lying states, such as the deeply bound $X\ ^1\Sigma^+$ state and the flat-bottomed $A\ ^1\Sigma^+$ state.[1] This aberrant behavior also appears in the $C\ ^1\Sigma^+$ state and develops a double-well potential, which is affected by the avoided crossing of electronic configurations with the same symmetry. Figure 1 shows the *ab initio* calculations of Ref. 2 of the four lowest $^1\Sigma^+$ states in solid blue lines and their diabatic curves are in dotted red lines. For adapting the avoided crossing of the diabatic interaction, these four $^1\Sigma^+$ states develop an irregular shape. Regarding the potential curve of the LiH $C\ ^1\Sigma^+$ state, which dissociates to Li(3s) + H(1s), a papillose inner potential well is formed due to the effect of the valence and Rydberg atomic configurations, and a major outer potential well is formed due to the interaction between the ionic and neutral electronic configurations.[3] The double-minimum potential commonly exists in the highly excited electronic states as can be seen in the example of LiH[4] and $Na_2$.[5] The calculated permanent dipole moments of the NaH $C\ ^1\Sigma^+$ state exhibits an irregular variation at the avoided crossing regions (2.5, 6.5, and 12.5 Å), which is a well-known magnification of the contribution of covalent and ion-pair electron wave functions.[6] The outer well potential curve of the NaH double-well $C\ ^1\Sigma^+$ state has been experimentally characterized using pulsed optical-optical double resonance (OODR) fluorescence depletion spectroscopy.[7]

In this study, an extended observation of the higher rovibrational levels ($v$ = 35–42, $J$ = 1–11; the highest observed rovibrational level is about 9 $cm^{-1}$ to its dissociation limit) of the NaH $C\ ^1\Sigma^+$ state is presented. These rovibrational levels are used to construct a hybrid double-well potential curve which can reproduce the eigenvalues within the experimental uncertainties. This hybrid potential curve is a modification of the combination of the Rydberg-Klein-Rees (RKR) potential curve of this work, the *ab initio* calculations, and a long-range potential. Additionally, the dissociation energy of the NaH $X\ ^1\Sigma^+$ state can be deduced from the determination of the dissociation limit of the NaH $C\ ^1\Sigma^+$ state.

## II. EXPERIMENT

The experimental setup is similar to that of the previous arrangement.[7] An Nd-YAG laser (Continuum Powerlite 8000, Santa Clara, USA) with 10 Hz pulse repetition rate, 5–7 ns pulse width, and 50 mJ/pulse was used to pump two wavelength-tunable dye lasers (Lambda Physik Scanmate II, Göttingen, Germany) that have 0.15 $cm^{-1}$ linewidth and an energy per pulse of 0.3–4.5 mJ. One of the dye lasers, pumped by the third harmonic of the Nd-YAG laser (355 nm), generates a violet PUMP (L1) laser beam to promote the NaH molecules from the $X\ ^1\Sigma^+$ state to the $A\ ^1\Sigma^+$ state. The methanol solution of laser dye (LC3990 or 400E) was used as an active medium and generated the desired laser energy for $X\ (v'' = 0, J'') \rightarrow A\ (v' = 7–8, J')$ transitions. Another dye laser, pumped by the second harmonic of the Nd-YAG laser (532 nm), generates a red PROBE (L2) laser beam to promote the NaH molecules from the $A\ ^1\Sigma^+$ state to the $C\ ^1\Sigma^+$ state. The 4-dicyanomethylene-2-methyl-6-(p-dimethylaminostyryl)-4H-pyran (DCM) laser

[a)]C.-C. Chu and H.-Y. Huang contributed equally to this work.
[b)]Authors to whom correspondence should be addressed: twhang@mail.ncku.edu.tw and chintsai@mail.ncku.edu.tw.

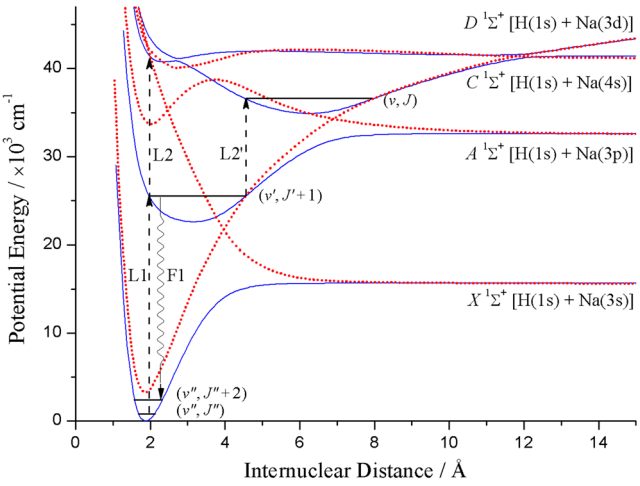


FIG. 1. The 4 lowest $^1\Sigma^+$ states of the NaH and the experimental scheme used to investigate the $C\ ^1\Sigma^+$ state (blue solid lines: adiabatic potential curves; red dotted lines: diabatic potential curves).

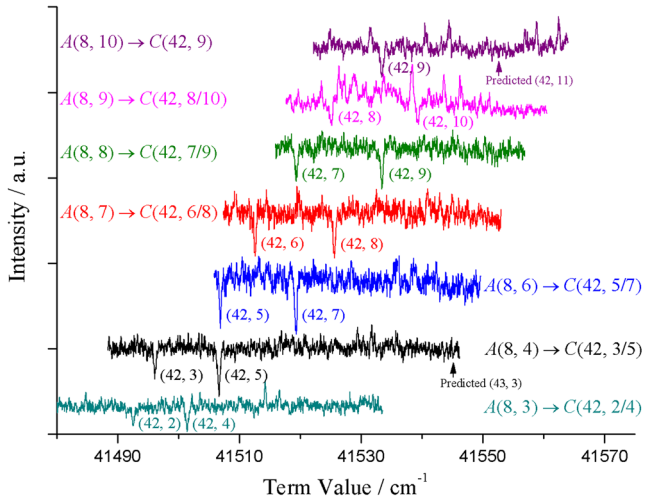


FIG. 2. OODR fluorescence depletion spectra, which shows that the rovibrational levels of the highest observed vibrational level $v = 42$ are observed from seven different intermediate $A$ states. The traces of the intermediate levels $A$ (8, 9) and $A$ (8, 10) are evidently affected by the $Na_2$ transitions of the higher excited triplet states back to the $a\ ^3\Sigma_u^+$ state.

dye was used for $A\ ^1\Sigma^+ \rightarrow C\ ^1\Sigma^+$ transitions in the spectral range 15 000–16 100 $cm^{-1}$. The iron and neon atomic lines from a Fe–Ne hollow cathode tube (Hamamatsu L233-26NU, Hamamatsu, Japan) were used to calibrate the frequency of the dye laser in the violet region. A molecular iodine cell at room temperature was used to calibrate the laser frequency in the visible region. The uncertainty of the frequency calibration is about 1.0 $cm^{-1}$ for both of the pump and probe lasers.

A five-arm stainless steel heat pipe was loaded with sufficient sodium metal filled with about 1 Torr of argon buffer gas. It was pre-purged with hydrogen gas and heated to about 410 °C to generate sodium hydride. The laser-induced fluorescence (LIF) from a state-selected transition back to the ground state was directed into a monochromator having 0.05 nm resolution (Acton Research Corporation SP-500, Acton, USA) and detected with a photomultiplier tube (Hamamatsu R928, Hamamatsu, Japan). The signal was processed with a boxcar integrator system (Stanford Research Systems SR245, SR250, and SR280, Sunnyvale, USA) and recorded on a personal computer.

The spectra were obtained using pulsed OODR fluorescence depletion spectroscopy. The electronic potential curves are shown in Fig. 1. The sodium hydride molecules are pumped by a fixed-frequency laser (L1) from the thermally populated ground state ($X\ ^1\Sigma^+$) to a state-selected excited state ($A\ ^1\Sigma^+$); moreover, a state-selected LIF (F1) is directed into a monochromator (a *PR* pair is usually used. *P* line: $\Delta J = -1$; *R* line: $\Delta J = +1$). The probe laser (L2 or L2′) is used to scan over the resonance range of a highly excited state ($C\ ^1\Sigma^+$). The intensity of LIF (F1) is maintained at a constant level because of the fixed-power PUMP laser; however, the depletion of F1 intensity takes place when the probe laser scans over a resonance.

## III. RESULTS

### A. Fluorescence depletion spectra

The OODR spectrum was detected by monitoring the fluorescence depletion of an *X*–*A* transition alternative to the *PR* pair of the pump laser, i.e., the monochromator detects the $A\ (v', J' + 1) \rightarrow X\ (v'', J'' + 2)$ fluorescence while the pump laser provides an $A\ (v', J' + 1) \leftarrow X\ (v'', J'')$ transition, or vice versa. Eighteen intermediate levels with $v' = 7$–8 and $J' = 2$–10 of the $A\ ^1\Sigma^+$ state were used in this study to probe the excited $C\ ^1\Sigma^+$ state. The assignment of the $A\ ^1\Sigma^+$ state is adopted from Ref. 8, and the absolute term energy for the intermediate levels is calibrated by the neon atomic lines.[9] The term value of each rovibrational level of the $C\ ^1\Sigma^+$ state was obtained by adding the energies of the intermediate *A* state and probe laser (L2 or L2′).

Figure 2 shows the fluorescence depletion spectra of the vibrational quantum levels near the dissociation limit of the *C* state. Successive rovibrational levels *C* (42, 2–10) were recorded via the intermediate levels *A* (8, 3–10). There are some fluorescence-enhanced peaks, e.g., on the traces of the intermediate level *A* (8, 9) or *A* (8, 10). This is due to the $Na_2$ transitions of the higher excited triplet Rydberg states back to the $a\ ^3\Sigma_u^+$ state (in the wavelength region of 350–450 nm).[10,11] The higher excited triplet Rydberg states of $Na_2$ were populated by the resonance-enhanced two-photon transitions and collision energy transfer under the probe laser L2 (or L2′).

Based on the recorded spectra, the highest observed vibrational quantum number in this work is $v = 42$. For each intermediate level, the transitions of *P* and *R* lines were observed except the intermediate level *A* (8, 10) which has only the *P* line of a *C* (42, 9) depletion signal. According to this observation, the highest observed rovibrational level of the *C* state near the dissociation limit [Na(4s) + H(1s)] is *C* (42, 10). The full width at half maximum (FWHM) of the *C* (42, *J*) spectral lines is around 0.5 $cm^{-1}$. There is no observable tunneling effect in the near-dissociation region.

### B. $v^*$ assignment

A total of 37 vibrational levels of the NaH $C\ ^1\Sigma^+$ state are observed. However, it is difficult to access the lowest 6

vibrational states ($v = 0$–5) because the equilibrium separation of the outer well of the $C\ ^1\Sigma^+$ state is almost twice of that of the $A\ ^1\Sigma^+$ state, as shown in Fig. 1. This phenomenon inhibits the Franck-Condon transition from the intermediate $A\ ^1\Sigma^+$ state ($v' = 7$–8), which is limited by exciting from the thermally populated $X\ ^1\Sigma^+$ state ($v'' = 0$), to the low-lying vibrational levels of the $C\ ^1\Sigma^+$ state. The proper Franck-Condon transition to access the bottom of the $C\ ^1\Sigma^+$ state is out of our laser capability.

By comparing the vibrational energy difference ($\Delta G_{v+1/2}$) between the theoretical calculations and the experimental data, the absolute vibrational quantum number of the $C\ ^1\Sigma^+$ state can be assigned. The observed rotational levels for each individual vibrational quantum state were fitted to a quadratic equation of the term values as a function of $J(J + 1)$ to obtain the rotation-less vibrational energy $G_v$. Numerically solving the Schrödinger equation with the theoretical potential curve,[6] the eigenvalues can be obtained and hence the $\Delta G_{v+1/2}$ of the $C\ ^1\Sigma^+$ state can be calculated for comparison with the corresponding experimental values.

The lowest 26 experimentally observed vibrational quantum levels (below the inner well) are involved for the comparison, i.e., a total of 25 vibrational energy differences are obtained. The average absolute difference $\delta\ \left(\delta = \frac{\sum|\Delta G_{v+1/2}(\text{expt.}) - \Delta G_{v+1/2}(\text{theo.})|}{n}\right)$ between the theoretical $\Delta G_{v+1/2}$(theo.) and the experimental $\Delta G_{v+1/2}$(expt.) is calculated, and a tentative assignment of the lowest observed vibrational quantum number $v^*$ is determined. Figure 3 shows the δ value versus tentative assignment $v^*$ according to Ref. 6 (red open circles). The error bar is the standard deviation of the δ for each tentatively assigned vibrational level. Follow the same procedure, the CI potential curve calculated by Olson and Liu[12] also illustrates the similar result (see Fig. 3, black open triangles). In Fig. 3, a larger δ value indicates a larger discrepancy between the theoretical potential and the experimental observation (see the supplementary material for details). The work of Aymar *et al.*[6] has smaller standard deviation and, therefore, the hybrid potential constructed in Sec. IV B is partially adopted from Ref. 6. Based on the analysis mentioned above, the lowest observed vibrational quantum number $v^*$ is assigned to 6.

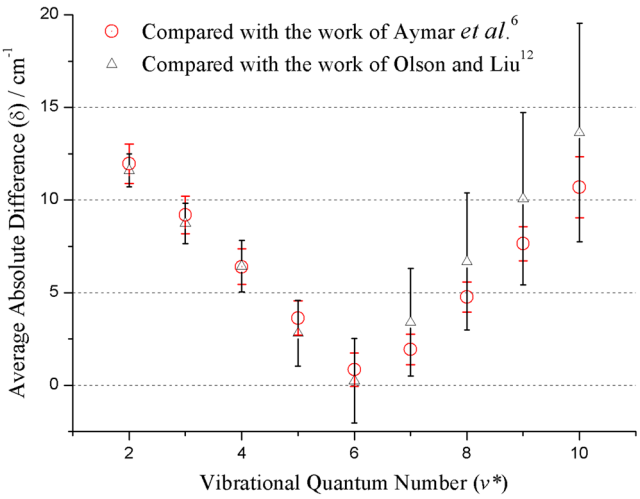


FIG. 3. The average absolute difference δ of $\Delta G_{v+1/2}$ versus tentative assignment $v^*$ (red open circles: compared with the work of Aymar *et al.*;[6] black open triangles: compared with the work of Olson and Liu[12]). The error bar is the standard deviation of each average absolute difference.

The assignment of the absolute vibrational quantum number of this work is off by one unit higher than the previous study[7] ($v^* = 5$). The key point is that after involving the newly observed data for analysis ($v > 34$ to the dissociation limit), we find that the NaH $C\ ^1\Sigma^+$ state potential modified from the work of Aymar *et al.*[6] will reproduce the eigenvalues in good agreement with the observed data, especially the levels above the inner-well potential which will be discussed later in Sec. IV B. Although the observed term values of the inner-well potential are identical, the bottom and the dissociation energy of the $C\ ^1\Sigma^+$ state will be re-defined after the re-assignment of the absolute vibrational quantum number ($v^* = 6$).

## IV. ANALYSIS

### A. Dunham coefficients

The observed data field of the NaH $C\ ^1\Sigma^+$ state contains 379 rovibrational levels ($v = 6$–42, $J = 1$–11) including a total of 602 transitions and is available in the supplementary material. There are some missing rotational levels in the higher vibrational levels due to the overwhelming perturbation background of the probe laser in the OODR spectrum. The OODR energy regime happens to be the red band absorption of $Na_2$ molecule $A\ ^1\Sigma_u^+ \leftarrow X\ ^1\Sigma_g^+$ transition. The $A$–$X$ band radiation extends from 570 to 830 nm and is responsible for the far wing of the self-broadened sodium D line.[13]

In order to make up the lowest unobserved 6 vibrational levels ($v = 0$–5), the eigenvalues derived from Ref. 6 are adopted in the analysis because the $\Delta G_{v+1/2}$ progression is well matched to our experimental results. Accordingly, these eigenvalues are altered by a constant shift for minimizing the difference between the experimental data and calculated term values. For the outer well of the NaH $C\ ^1\Sigma^+$ state, 456 experimental data ($v = 6$–34, $J = 1$–11) along with 18 eigenvalues ($v = 0$–5, $J = 0$, 5, and 10) derived from theoretical calculation are adopted to obtain a set of Dunham coefficients. Three chosen $J$ values are due to the reduction in the influence of unobserved levels, and the maximum $J = 10$ is to cover the experimental observations. A total of 12 terms are used in the Dunham fitting, and the Dunham expansion is shown as follows:[14,15]

$$\begin{aligned} T(v,J) &= G(v) + F_v(J) \\ &= \left[\omega_e\left(v+\frac{1}{2}\right) - \omega_e x_e\left(v+\frac{1}{2}\right)^2 + \cdots\right] \\ &\quad + \left[B_v J(J+1) - D_v J^2(J+1)^2 + \cdots\right] \\ &= \sum_{i=0}^{\infty}\sum_{j=0}^{\infty} Y_{ij}\left(v+\frac{1}{2}\right)^i [J(J+1)]^j. \end{aligned} \tag{1}$$

Table I presents the Dunham coefficients of the NaH $C^1\Sigma^+$ state, and the standard deviation of the average error between the fitted and observed values is 0.24 cm$^{-1}$, which is within the experimental error. (Note that the number of significant digits in Table I does not indicate the experimental precision

TABLE I. Dunham coefficients of the NaH $C\ ^1\Sigma^+$ state based on the lowest observed vibrational quantum number $v^* = 6$ (experimental observations are for $v = 6$–34 and $J = 1$–11). All values are in $cm^{-1}$.

| | |
|---|---|
| $T_e$ | 34952.77 ± 0.17 |
| $Y_{00}$ | −0.441 3 ± 0.0060 |
| $Y_{10}$ | 218.599 486 2 ± 0.1041 |
| $Y_{20}$ | −1.847 798 289 ± 0.0233 |
| $Y_{30} \times 10^2$ | 2.811 369 180 ± 0.2337 |
| $Y_{40} \times 10^3$ | −1.013 643 367 ± 0.1156 |
| $Y_{50} \times 10^5$ | 1.995 986 269 ± 0.2769 |
| $Y_{60} \times 10^7$ | −1.535 209 688 ± 0.2566 |
| $Y_{01}$ | 0.472 346 884 ± 0.0020 |
| $Y_{11} \times 10^3$ | 3.563 786 976 ± 0.3653 |
| $Y_{21} \times 10^4$ | −1.331 840 715 ± 0.2213 |
| $Y_{31} \times 10^6$ | 3.143 545 024 ± 0.3996 |
| $Y_{02} \times 10^5$ | −5.754 988 761 ± 0.7742 |

but rather to maintain the calculation round-off.) The Dunham coefficients are used to construct an RKR potential curve for the vibrational levels $v$ = 0–34. Details of the Dunham fitting and RKR potential curve can be found in the supplementary material. However, the traditional method of solving the potential curve cannot effectively obtain a double-well potential. Fortunately, there is another way to overcome this problem.

### B. Hybrid potential

Several higher rovibrational levels ($v > 34$) having different physical behaviors in comparison with the harmonic potential region ($v$ = 0–34), such as $\Delta G_{v+1/2}$, still remain to be dealt with. To derive the irregular vibrational constant for the levels above the double-well, the rotational levels associated with each vibrational level are substituted into $G(v) = G_v + B_v J(J + 1)$ to yield the corresponding vibrational ($G_v$) and rotational ($B_v$) constants. Figure 4 plots the $\Delta G_{v+1/2}$ of each vibrational level (blue open circles) and reveals three regions of variation of $\Delta G_{v+1/2}$ (see the supplementary material for details). For $v$ = 0–34 with harmonic variation, it reveals that

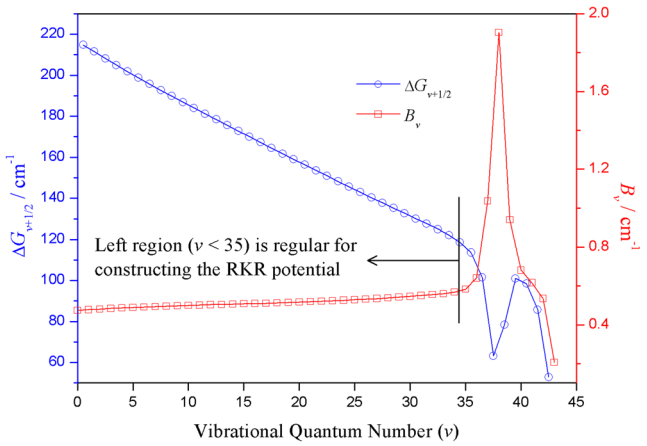


FIG. 4. Vibrational energy difference $\Delta G_{v+1/2}$ (blue open circles) and rotational constant $B_v$ (red open squares) of the NaH $C\ ^1\Sigma^+$ state. The blue and red solid lines are for the sake of clear demonstration of the variation.

the regular interaction between covalent and ionic potential and shows a linear decreasing of $\Delta G_{v+1/2}$. This region is suitable for the Dunham expression and the construction of the RKR potential, as discussed in Sec. IV A (Dunham coefficients and the RKR potential are available). For $v$ = 40–43 ($v$ = 43 is expected from solving the Hamiltonian of the hybrid potential), the $\Delta G_{v+1/2}$ variation has a sharp bending that reveals the near dissociation characteristics of long-range atom-atom interactions. In analogy to the LiH $C\ ^1\Sigma^+$ state,[3] an inner well in the region of $v$ = 35–39 owing to the ionic-covalent avoided crossing arises a V-type variation of $\Delta G_{v+1/2}$.

According to the formula of rotational constant $B = h/8c\mu\pi^2 r^2$, the vibrational level in the inner well will have a larger rotational constant than that in the outer well because the rotational constant is inversely proportional to the square of the internuclear distance, as shown in Fig. 4 (red open squares). The vibrational levels affected by the inner well are spread around $v$ = 35–39, in which the smallest $\Delta G_{v+1/2}$ value is 61.15 $cm^{-1}$ for $v$ = 37 and the largest $B_v$ value is 1.902 $cm^{-1}$ for $v$ = 38.

In general, the dissociation limit can be deduced from the long-range behavior. However, the last 3 points of the $\Delta G_{v+1/2}$ decrease too fast to present the long-range behavior because the energy gap difference between each of the last 3 successive vibrational levels is huge, which is different from the homo-nuclear diatomic molecule such as $Na_2$. In this work, the outer turning point of the highest observed vibrational level ($v$ = 42) is still within the Le Roy radius $R_{LR}$ = 13.7 Å, which characterizes the internuclear distance showing no long-range behavior. This is a typical situation for alkali hydrides. To obtain a complete hybrid potential of the NaH $C\ ^1\Sigma^+$ state which can represent the variation of these rovibrational levels, the inverted perturbation analysis (IPA) method[16] was used. The hybrid potential was constructed from five regions of different internuclear distances ($R$) as shown in Table II. Region I is a modified potential adopted from the theoretical potential[6] for short internuclear distances $R < R_{min}$ ($v$ = 42); region II includes the inner well potential in the range of $R_{min}$ ($v$ = 42) $< R < R_{min}$ ($v$ = 34); region III is the RKR potential and covers the range of $R_{min}$ ($v$ = 34) $< R < R_{max}$ ($v$ = 34) which will be discussed later; region IV is a modified potential adopted from the theoretical potential[6] for long internuclear distances $R_{max}$ ($v$ = 34) $< R < R_{LR}$ = 13.7 Å; region V is the long-range potential reported by Proctor and Stwalley[17] with $R$ > 13.7 Å. In regions I, II, and IV, the modification is based on the theoretical potential reported by Aymar *et al.*[6]

The modification of region I is a scale shift of the decrease of the internuclear distance and the increase of potential energy to connect with the RKR potential inner well. In region II, the experimental $\Delta G_{v+1/2}$ has five vibrational levels affected by the inner well and the smallest $\Delta G_{v+1/2}$ value is 61.15 $cm^{-1}$ for vibrational level $v$ = 37, whereas the eigenvalues derived from the theoretical potential[6] have only four vibrational levels affected by the inner well and the smallest $\Delta G_{v+1/2}$ is 75.27 $cm^{-1}$ for $v$ = 36. Besides, the separation of the rotational energy levels is given by $\Delta F_v(J) = F_v(J + 1) - F_v(J)$, which also shows the following differences: the experimental $\Delta F_v(J)$ for $v$ = 38, $J$ = 0–6 is larger and $\Delta F_v(J)$ for $v$ = 37,

TABLE II. The hybrid potential of the NaH $C\ ^1\Sigma^+$ state. $R_{min}$ ($v$ = 42) represents the inner turning point of the highest observed vibrational level $v$ = 42. $R_{min}$ ($v$ = 34) and $R_{max}$ ($v$ = 34) represent the inner and outer turning points of the vibrational level $v$ = 34, which is the highest vibrational level of the outer well. The long-range region starts from the Le Roy radius $R_{LR}$ = 13.7 Å.

| Region | $R$ | $U(R)$ | Reference |
|---|---|---|---|
| I | $R < R_{min}$ ($v$ = 42) | *ab initio* | 6 |
| II | $R_{min}$ ($v$ = 42) < $R$ < $R_{min}$ ($v$ = 34) | *ab initio* | 6 |
| III | $R_{min}$ ($v$ = 34) < $R$ < $R_{max}$ ($v$ = 34) | RKR potential | This work |
| IV | $R_{max}$ ($v$ = 34) < $R$ < 13.7 Å | *ab initio* | 6 |
| V | 13.7 Å < $R$ | $C_6R^{-6}$–$C_8R^{-8}$–$C_{10}R^{-10}$ | 17[a] |

[a]The long-range coefficients ($C_n$) are $C_6$ = 550.4, $C_8$ = 152 200, and $C_{10}$ = 49 960 000, all in units [cm$^{-1}$ Å$^n$].

$J$ = 0–6 is smaller than that calculated from the theoretical potential. These results reveal that the real inner well should be with a deeper depth and higher barrier than that of the theoretical potential. After modification, the inner well is located between $R_{min}$ = 2.08 Å and 2.67 Å.

In region IV, the hybrid potential curve is modified from the theoretical potential in order to connect to the RKR potential curve and to fit the $\Delta F_v(J)$ variation in the rovibrational levels $v$ > 34 and $J$ > 6. In region V, the potential is governed by the long-range behavior and can be presented by the long-range expansion ($V_{long\text{-}range}(R) = -\Sigma C_n/R^n$) along with the long-range coefficients $C_6$ = 550.4, $C_8$ = 152 200, and $C_{10}$ = 49 960 000, all in units [cm$^{-1}$·Å$^n$], taken from Ref. 17. The complete hybrid potential is shown in Fig. 5 and its details can be found in the supplementary material. The RKR potential (red solid circles) constructed from the Dunham coefficients has an outer well equilibrium nuclear distance $R_e$ = 6.08 Å. The hybrid potential (red solid line) has an inner well equilibrium nuclear distance $R_e$ = 2.34 Å. The vertical dashed-dotted line shows the Le Roy radius ($R_{LR}$ = 13.7 Å), which is the criterion for the starting radius of the long-range behavior. The definition of the Le Roy radius is $R_{LR} = 2[\langle r_{Na}{}^2\rangle^{1/2} + \langle r_H{}^2\rangle^{1/2}]$, where the $\langle r_{Na}{}^2\rangle$ and $\langle r_H{}^2\rangle$ are the expectation values of the square of the radius of atoms Na(4s) and H(1s), respectively.[17–20] The *ab initio* potential energy curve[6] is also shown in Fig. 5 with blue dotted line, which has an outer well at $R_e$ = 6.22 Å with $D_e$ = 6501 cm$^{-1}$ and an inner well at $R_e$ = 2.35 Å with $D_e$ = 661 cm$^{-1}$. Note that the *ab initio* curve in Fig. 5 has been translated to meet the asymptote Na(4s) + H(1s).

The inset of Fig. 5 shows the enlarged long-range region of the NaH $C$ state. The open red circles represent the $G_v$ derived from the hybrid potential and the open triangle represents the predicted $G_v$ of the highest vibrational level $v$ = 43 which was not observed in this work. The highest predicted level is weakly bound (bound by only ~6 cm$^{-1}$) and is too close to the dissociation limit for spectroscopic observation.

The eigenvalues and eigenfunctions of the NaH $C\ ^1\Sigma^+$ state can be obtained by solving the Hamiltonian with the hybrid potential curve constructed in this work. These eigenvalues are plotted in Fig. 6 as a function of $J(J + 1)$ and the details are available in the supplementary material. Figure 6 shows the experimental data (solid black circles), the eigenvalues derived from the RKR potential (blue crosses), the eigenvalues derived from the hybrid potential (red open circles; red solid lines are for the connection of each vibrational level),

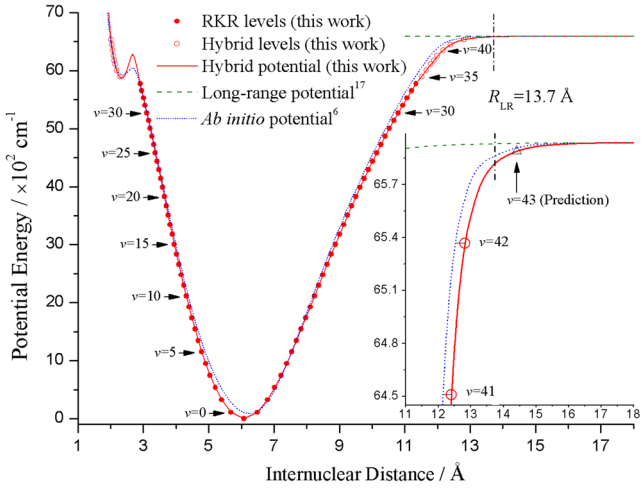


FIG. 5. The hybrid, RKR, and long-range potentials of the NaH $C\ ^1\Sigma^+$ state [red solid circles: the RKR rotation-less levels; red open circles: the hybrid rotation-less levels; red solid line: the hybrid potential energy curve; green dashed line: the long-range potential energy curve (Ref. 17); blue dotted line: the *ab initio* potential energy curve (Ref. 6); black dashed-dotted line: the Le Roy radius (Ref. 20)]. Inset: An enlarged scale of the long-range region, which reveals that the predicted level $v$ = 43 is close to the dissociation limit.

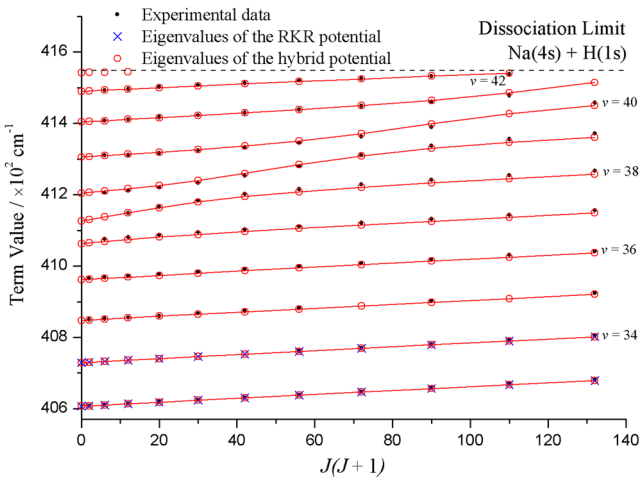


FIG. 6. The near-dissociation region of term values vs. $J(J + 1)$, including the avoided crossing region [black solid circles: the experimental observed term values; blue crosses: the eigenvalues derived from the RKR potential; red open circles: the eigenvalues derived from the hybrid potential; black dashed line: the dissociation limit to Na(4s) + H(1s)].

and the rotation-less dissociation limit (black dashed line) of Na(4s) + H(1s). The average discrepancies between the eigenvalues derived from the hybrid potential and the experimental term values are 0.55 $cm^{-1}$ in $v$ = 6–34 (RKR region) and 1.93 $cm^{-1}$ in $v$ = 35–42 (hybrid region). The latter discrepancy is mainly from the inner well regime. Overall, the tendency affected by the inner well matches well with the experimental observations, which supports the reliability and validity of the hybrid potential curve constructed in this work.

In Fig. 6, each of the connected lines for the vibrational quantum number $v < 35$ shows a high linearity. However, the connected line starts to bend for $v$ = 36–41. The clear bending points occur at $J$ = 5 ($v$ = 38), $J$ = 5 and 8 ($v$ = 39), $J$ = 8 and 10 ($v$ = 40), and $J$ = 10 ($v$ = 41) separately, which provides the evidence of the existence of the inner well. The bending phenomenon can also be presented by the variation of $\Delta G_{v+1/2}(J)$ as shown in Fig. 7. This figure plots the $\Delta G_{v+1/2}$ with respect to different rotational quantum numbers versus the vibrational quantum number; it reveals that the energy difference is changing with the rotational quantum number (see the supplementary material for details).

With regard to the $C\ ^1\Sigma^+$ state of LiH, the vibrational bending of NaH is not that dramatic. According to the literature reported by Chen and co-workers,[3] the LiH molecule can be stably trapped in the inner well. Once the molecule is trapped, the probability density is dominantly present in the inner well. In order to understand the relevant behavior of the NaH $C\ ^1\Sigma^+$ state, the wave function squared, i.e., the probability density of different rovibrational levels derived from the hybrid potential is calculated and plotted in Fig. 8. This figure shows the probability density for the five rotation-less levels with the solid red ($v$ = 34, 36, 40, and 42) and blue ($v$ = 38) lines (see the supplementary material for details). For the levels $C$ (34, 0) and $C$ (36, 0), the probability density is mainly located between the internuclear distance of the outer well (~3–11 Å) and seems not obviously affected by the inner well. For the level $C$ (38, 0), the probability density is affected by the inner well and it shows higher probabilities at the short internuclear distance (~2–3 Å); however, the energy level $C$ (38, 10) is higher than the inner well barrier so that the probability density transfers to the longer internuclear distance (~3–12 Å). For the vibrational levels $v$ = 40 and 42, the molecule is also affected by the inner well because the probability density distributes over the inner and outer well region.

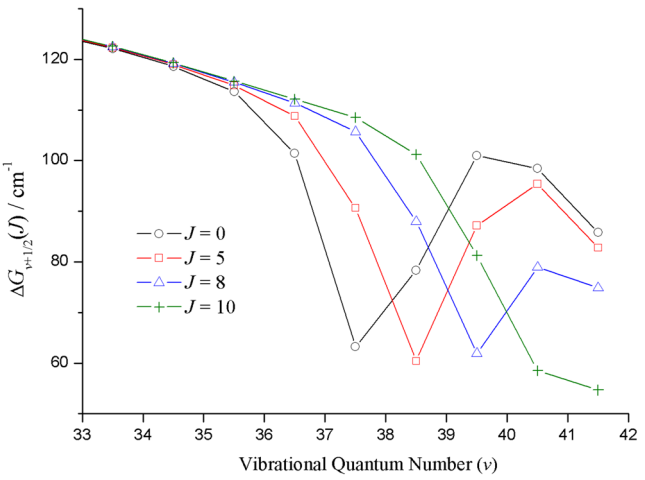


FIG. 7. The vibrational energy difference for different rotational quantum number $\Delta G_{v+1/2}(J)$ vs. vibrational quantum number $v$ (black open circles: $J$ = 0; red open squares: $J$ = 5; blue open triangles: $J$ = 8; green pluses: $J$ = 10).

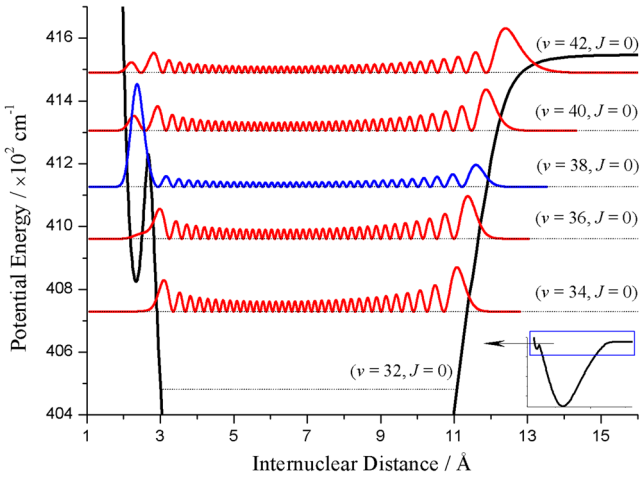


FIG. 8. Probability density of five rotation-less levels of the near-dissociation region ($v$ = 34, 36, 38, 40, and 42), including the avoided crossing region. The vibrational level $v$ = 38 (blue solid line) is unambiguously affected by the inner well.

The population of the probability density of the NaH $C\ ^1\Sigma^+$ state distributes over the inner and outer well in comparison with the LiH $C\ ^1\Sigma^+$ state. This phenomenon reveals that the inner well of the NaH $C\ ^1\Sigma^+$ state is too shallow to trap the molecule and can just affect the nearby rovibrational levels.

### C. Dissociation energy of the $C\ ^1\Sigma^+$ and $X\ ^1\Sigma^+$ state

To determine the dissociation energy of the NaH $C\ ^1\Sigma^+$ state, the hybrid potential is slightly modified by adding a constant energy of −0.5, −1, +1, and +2 $cm^{-1}$ to the energy of the depth of the potential well (dissociation limit) to obtain the eigenvalues of the highest vibrational level and then to compare with the corresponding experimental values (see the supplementary material for details). Each modified hybrid potential will obtain a sum of the difference between the eigenvalue and the experimental value and the corresponding standard deviation, as shown in Fig. 9. The dissociation energy of the NaH $C\ ^1\Sigma^+$ state can be estimated by fitting a linear regression to five points of the difference (1 original and 4 modified dissociation energies). It gives the dissociation energy of the outer well $D_e = 6595.10 \pm 5$ $cm^{-1}$ and the inner well $D_e = 723.64 \pm 5$ $cm^{-1}$. The uncertainty mainly arises from the laser calibration and slightly from the fitting error.

According to the previous report,[21] the dissociation energy of the NaH $X\ ^1\Sigma^+$ state is estimated by means of the Birge-Sponer extrapolation method along with the highest observed vibrational level ($v'' = 21$) near the dissociation limit. In Fig. 4, the sharp slope of the $\Delta G_{v+1/2}$ variation for the last three points reveals that the highest observed vibrational level is much closer to the dissociation limit. Besides,

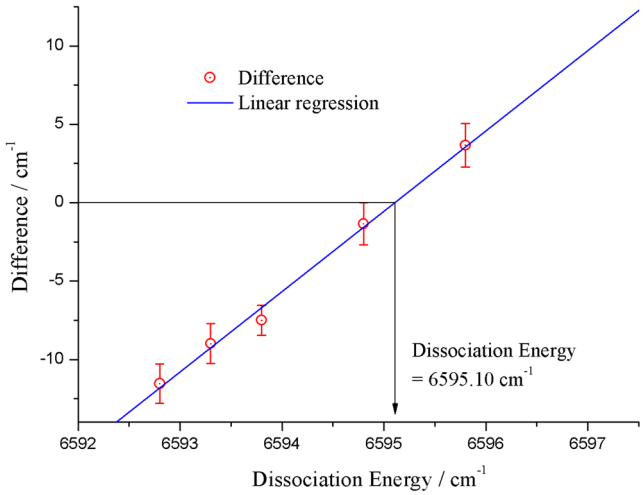


FIG. 9. Interpolation of the dissociation energy of the NaH $C\ ^1\Sigma^+$ state (red open circles: the summation of the difference between the eigenvalues and the experimental values; blue solid line: linear regression of these five difference points). The zero difference point marked by a horizontal line indicates that the dissociation energy $D_e(C)$ is 6595.10 $cm^{-1}$.

the derivation of the dissociation energy of the NaH $C\ ^1\Sigma^+$ state is independent of the dissociation energy of the $X\ ^1\Sigma^+$ state. In other words, the dissociation energy of the NaH $X\ ^1\Sigma^+$ state can be evaluated by using the relation $D_e(X) = D_e(C) + T_e(C) - \Delta E(\text{Na } 4s–3s)$. The $T_e$ = 34 952.77 $cm^{-1}$ is derived from the experimental data; the $\Delta E$(Na 4s–3s) is 25 739.999 $cm^{-1}$ for the atomic energy difference between the sodium energy levels of 3s and 4s;[22] the $D_e(C)$ is 6595.10 $cm^{-1}$ from this work. Accordingly, the dissociation energy of the NaH $X\ ^1\Sigma^+$ state is 15 807.87 ± 5 $cm^{-1}$, which is consistent with the experimental value of 15 815 ± 5 $cm^{-1}$ derived from experimental near-dissociation energy levels of the NaH $X$ state.[21]

## V. CONCLUSIONS

In this work, 379 rovibrational levels ($v$ = 6–42, $J$ = 1–11) of the NaH $C\ ^1\Sigma^+$ state up to the dissociation limit [Na(4s) + H(1s)] are observed by pulsed OODR fluorescence depletion spectroscopy. The highest observed rovibrational level is $C$ (42, 10) which covers more than 99.9% of the well-depth. A set of Dunham coefficients is deduced to describe the outer well of the NaH $C\ ^1\Sigma^+$ state including the lower vibrational levels $v$ = 0–34 ($v$ = 0–5 is adopted from *ab initio* calculation[6]). A complete hybrid double-well potential curve is constructed to reproduce the irregular rovibrational progressions. The illustration of the term values versus $J(J + 1)$ shows an irregular variation of the vibrational and rotational constants around the inner well regime. This hybrid potential should be reliable because the eigenvalues derived from the hybrid potential are in good agreement with the observations. The illustration of the probability density of the five rotation-less levels reveals that the inner well is too shallow to trap the atoms; however, the existence of the inner well indeed has influence upon the nearby rovibrational levels. A linear regression approach is used to evaluate the dissociation energy $D_e$ of the NaH $C\ ^1\Sigma^+$ state by modifying the energy of the dissociation limit. Finally, according to the dissociation energy of the $C\ ^1\Sigma^+$ state, the dissociation energy of the $X\ ^1\Sigma^+$ state is also discussed and evaluated in this work.

## SUPPLEMENTARY MATERIAL

See supplementary material for the (1) determination of absolute vibrational quantum number; (2) observed transitions and rovibrational term values of this work; (3) Dunham fitting output of the NaH $C\ ^1\Sigma^+$ state; (4) RKR potential curve for the NaH $C\ ^1\Sigma^+$ state; (5) comparison of the vibrational constants; (6) data of $T_{v,j}$ vs. $J(J + 1)$; (7) hybrid potential curve for the NaH $C\ ^1\Sigma^+$ state; (8) vibrational and rotational constants with different $J$; (9) FCFs for the NaH $A$–$C$ transition; (10) interpolation of dissociation energies; (11) wave function and probability density (normalized) for $v$ = 34, 36, 38, 40, 42 with $J$ = 0, 5, 10; and (12) effective potential and the linewidth analysis of the NaH $C\ ^1\Sigma^+$ state for the vibrational level $v$ = 42.

## ACKNOWLEDGMENTS

We gratefully acknowledge the support of the Ministry of Science and Technology, Taiwan under Grant Nos. NSC 100-2113-M-006-005 and NSC 102-2113-M-006-011. Chia-Ching Chu acknowledges the careful reading and helpful suggestions on details of the paper provided by Rui-En Hsu.

[1] W. C. Stwalley, W. T. Zemke, and S. C. Yang, J. Phys. Chem. Ref. Data **20**, 153 (1991).
[2] N. Khelifi, J. Phys. Chem. A **113**, 8425 (2009).
[3] J. J. Chen, W. T. Luh, and G. H. Jeung, J. Chem. Phys. **110**, 4402 (1999).
[4] A. Yiannopoulou, G. H. Jeung, S. J. Park, H. S. Lee, and Y. S. Lee, Phys. Rev. A **59**, 1178 (1999).
[5] D. L. Cooper, R. F. Barrow, J. Vergès, C. Effantin, and J. d'Incan, Can. J. Phys. **62**, 1543 (1984).
[6] M. Aymar, J. Deiglmayr, and O. Dulieu, Can. J. Phys. **87**, 543 (2009).
[7] H. Y. Huang, Y. Y. Chang, M. H. Liao, K. L. Wu, T. L. Lu, Y. Y. Chang, C. C. Tsai, and T. J. Whang, Chem. Phys. Lett. **493**, 53 (2010).
[8] F. P. Pesl, S. Lutz, and K. Bergmann, Eur. Phys. J. D **10**, 247 (2000).
[9] E. B. Saloman and C. J. Sansonetti, J. Phys. Chem. Ref. Data **33**, 1113 (2004).
[10] Z. G. Wang, L. A. Ma, H. R. Xia, K. C. Zhang, and I. S. Cheng, Opt. Commun. **58**, 315 (1986).
[11] L. Li and R. W. Field, J. Mol. Spectrosc. **117**, 245 (1986).
[12] R. E. Olson and B. Liu, J. Chem. Phys. **73**, 2817 (1980).
[13] L. K. Lam, T. Fujimoto, A. C. Gallagher, and M. M. Hessel, J. Chem. Phys. **68**, 3553 (1978).
[14] J. L. Dunham, Phys. Rev. **41**, 721 (1932).
[15] G. Herzberg, *Molecular Spectra and Molecular Structure*, Spectra of Diatomic Molecules (Robert E. Krieger Publishing Co., Malabar, FL, 1989), Vol. 1.
[16] I. P. Hamilton, J. C. Light, and K. B. Whaley, J. Chem. Phys. **85**, 5151 (1986).
[17] T. R. Proctor and W. C. Stwalley, J. Chem. Phys. **66**, 2063 (1977).
[18] W. T. Zemke, R. E. Olson, K. K. Verma, W. C. Stwalley, and B. Liu, J. Chem. Phys. **80**, 356 (1984).
[19] W. T. Zemke, R. E. Olson, K. K. Verma, W. C. Stwalley, and B. Liu, J. Chem. Phys. **85**, 4209 (1986).
[20] R. J. Le Roy, Can. J. Phys. **52**, 246 (1974).
[21] H. Y. Huang, T. L. Lu, T. J. Whang, Y. Y. Chang, and C. C. Tsai, J. Chem. Phys. **133**, 044301 (2010).
[22] J. E. Sansonetti, J. Phys. Chem. Ref. Data **37**, 1659 (2008).